View metadata, citation and similar papers at core.ac.uk

brought to you by CORE

provided by DigitalCommons@University of Nebraska

University of Nebraska - Lincoln
DigitalCommons@University of Nebraska - Lincoln

Papers in the Earth and Atmospheric Sciences | Earth and Atmospheric Sciences, Department of

2017

Fire and Smoke Remote Sensing and Modeling Uncertainties: Case Studies in Northern Sub-Saharan Africa

Charles Ichoku
NASA Goddard Space Flight Center

Luke T. Ellison
NASA Goddard Space Flight Center

Yun Yue
University of Nebraska - Lincoln

Jun Wang
University of Iowa

Johannes W. Kaiser
Max Planck Institute for Chemistry

Follow this and additional works at: http://digitalcommons.unl.edu/geosciencefacpub


Part of the Earth Sciences Commons

Ichoku, Charles; Ellison, Luke T.; Yue, Yun; Wang, Jun; and Kaiser, Johannes W., "Fire and Smoke Remote Sensing and Modeling Uncertainties: Case Studies in Northern Sub-Saharan Africa" (2017). *Papers in the Earth and Atmospheric Sciences*. 495.
http://digitalcommons.unl.edu/geosciencefacpub/495

This Article is brought to you for free and open access by the Earth and Atmospheric Sciences, Department of at DigitalCommons@University of Nebraska - Lincoln. It has been accepted for inclusion in Papers in the Earth and Atmospheric Sciences by an authorized administrator of DigitalCommons@University of Nebraska - Lincoln.

14

Fire and Smoke Remote Sensing and Modeling Uncertainties: Case Studies in Northern Sub-Saharan Africa

Charles Ichoku,[1] Luke T. Ellison,[2] Yun Yue,[3] Jun Wang,[3,4] and Johannes W. Kaiser[5]

ABSTRACT

Significant uncertainties are incurred in deriving various quantities related to biomass burning from satellite measurements at different scales, and, in general, the coarser the resolution of observation the larger the uncertainty. WRF-Chem model simulations of smoke over the northern sub-Saharan African (NSSA) region for January–February 2010, using fire energetics and emissions research version 1.0 (FEERv1) aerosol emissions derived from MODIS measurements of fire radiative power (FRP) and aerosol optical depth (AOD), resulted in a severe model underestimation of AOD compared with satellite retrievals. Such uncertainties are attributable to three major factors: limitations in the spatial and temporal resolutions of the satellite observations used to quantify emissions, modeling parameters and assumptions, and the unique geographic characteristics of NSSA. It is recommended that field campaigns involving synergistic coordination of ground-based, airborne, and satellite measurements with modeling be conducted in major and complex biomass burning regions such as the NSSA, and that significant improvements in the spatial and temporal resolutions of observation systems needed to reduce uncertainties in biomass burning characterization be seriously considered in future satellite missions.

14.1. INTRODUCTION

Wildfires and other types of open biomass burning represent one of the most ubiquitous disturbances to vegetated land ecosystems globally [e.g., *Andreae*, 1991; *Ichoku et al*., 2008a, 2012]. These vegetation fires are either ignited by natural processes such as lightning or by human action such as arson, accident, prescribed (controlled) burning for land management, or societal cultural practices as applicable to game hunting, slash-and-burn agriculture, and other forms of land clearing. Whatever the nature or purpose of ignition, depending on circumstances, such open fires can easily become hazardous to life and property. The hazardous effects of fires are not limited to the destructive effects of the associated flame and heat [e.g., *Cohen*, 2010], but also extend to the potential adverse impacts of the emitted smoke on air quality and human health both near and far [e.g., *Colarco et al*., 2004; *Wang et al*., 2006; *Wiedinmyer et al*., 2006; *Henderson et al*., 2011], as well as those of the postburn land surface processes that may include erosion, landslides, mud deposits, and pollution of water resources by soot and other residues [e.g., *Moody et al*., 2013].

Determination of the areas and quantities of biomass consumed by fires, and their resulting emissions and impacts, can be done at local to global scales, depending on the targeted application(s) and the available tools and resources [e.g., *Michalek et al*., 2000; *Ichoku and Kaufman*, 2005; *Roberts et al*., 2005; *van der Werf et al*., 2006, 2010; *de Groot et al*., 2007; *Pouliot et al*., 2008; *Schultz et al*., 2008; *Vermote et al*., 2009; *Giglio et al*., 2010; *Roy et al*.,

[1]*Climate and Radiation Laboratory, NASA Goddard Space Flight Center, Greenbelt, Maryland, USA*

[2]*Climate and Radiation Laboratory, NASA Goddard Space Flight Center, Greenbelt, Maryland, and Science Systems and Applications Inc., Lanham, Maryland, USA*

[3]*Department of Earth and Atmospheric Sciences, University of Nebraska, Lincoln, Nebraska, USA*

[4]*Now at Center for Global and Regional Environmental Research, and Department of Chemical and Biochemical Engineering, University of Iowa, Iowa City, Iowa, USA*

[5]*Max Planck Institute for Chemistry, Mainz, Germany*

Natural Hazard Uncertainty Assessment: Modeling and Decision Support, Geophysical Monograph 223, First Edition.
Edited by Karin Riley, Peter Webley, and Matthew Thompson.
© 2017 American Geophysical Union. Published 2017 by John Wiley & Sons, Inc.

This document is a U.S. government work and is not subject to copyright in the United States.

2010; *French et al*., 2011; *Kaiser et al*., 2012; *Miettinen et al*., 2013; *Peterson and Wang*, 2013; *Peterson et al*., 2013; *Ichoku and Ellison*, 2014; *Schroeder et al*., 2014a]. Irrespective of the approach or scale, such exercises are generally associated with a wide range of uncertainties, which are partly because of the dynamic and intractable nature of biomass burning processes, and partly due to the imperfections in the measurement approaches and modeling assumptions used. Measurement methods may be ground based, airborne, or satellite based. Ground-based methods are typically used for localized measurements with high precision over a short time period, whereas satellite methods can be applied regionally or globally for an extended time period albeit with a lower accuracy and precision. Based on the analysis of burned areas retrieved from multiple satellite sensors during 1997–2008, it was estimated that between 330 and 430 Mha were burned annually globally, of which ~250 Mha (i.e., ~70%) was estimated to have burned each year on the continent of Africa alone [*Giglio et al*., 2010]. These numbers were used, within the Global Fire Emissions Database version 3 (GFED3) framework, to estimate that the global annual carbon emissions from open biomass burning for 1997–2009 was in the range of 1.6 Pg C yr^{-1} to 2.8 Pg C yr^{-1}, with an annual average of 2.0 Pg C yr^{-1}, of which Africa alone contributes ~52% [*van der Werf et al*., 2010]. Although the emission uncertainties associated with such satellite-based global estimates are large, they can be even larger at regional scales. For instance, *Zhang et al*. [2014] found a factor of 12 difference when comparing seven satellite-derived fire emissions inventories for February 2010 in the northern sub-Saharan African (NSSA) region. Therefore, although the current paper will examine these uncertainties from a global perspective, case studies will be mainly based on data from the NSSA region, which comprise mostly savanna fires [e.g., *Gatebe et al*., 2014].

Some of the main uncertainties in quantifying biomass burning parameters stem from a variety of factors, including the difficulty in addressing the following questions: (1) Where and when exactly does a fire occur? (2) What are the mass loadings and conditions of the biomass fuel? (3) What is the fire intensity and/or size? (4) What are the relative proportions of the fire phases (flaming, smoldering, and glowing) per unit area and how does this distribution vary in space and time? (5) How long does a given fire burn, and how does it affect (and is it affected by) environmental conditions? (6) How far does a given fire spread, when is an area considered burned, and what is the total burned area when the fire ends? (7) How much smoke is emitted per unit time from a given fire? (8) How high is the plume injected and how far is it spreading? (9) What are the important constituents of the smoke and what are their respective concentrations? (10) How do smoke constituents interact with one another and with other atmospheric constituents to change and/or form new ones over time? (11) How do the characteristics of different fires in similar ecosystems differ? (12) What are the fire diurnal cycle and the seasonal burn pattern in a given area or region?

These questions are not an exhaustive list of the essential questions concerning the quantification of biomass burning characteristics and emission constituents. Yet no single measurement or modeling approach can address any of them to the required accuracy at various spatial and temporal scales. For instance, although ground-based and airborne systems can be used for limited active fire measurements at high temporal frequency over an extended part of a day, only portions of the fire or smoke can be observed at any given time. Conversely, satellite measurements can cover much larger regions or even the entire globe, but only for a smaller set of parameters at a much reduced spatial resolution and/or temporal frequency, depending on whether the satellite is geostationary or polar orbiting. Ideally, the ability to address most of the above questions to an acceptable level of accuracy should involve proper synergy between the different (ground-based, airborne, and satellite) measurement approaches and appropriate modeling systems [e.g., *Schroeder et al*., 2014a].

This study addresses uncertainties related to the satellite approach, which has become more and more widely used for fire characterization and emissions estimation at local to global scales. It is recognized that satellite observation systems are numerous and varied, thereby offering a similarly diverse range of capabilities for remote sensing of fires and smoke. However, the pyrolysis and emissions processes of biomass burning are extremely dynamic and continuous, and cannot be adequately followed by satellite observations, which can only provide highly discretized and sparse (both spatially and temporally) sampling of such processes. This gap in observation resulting from the intrinsic sampling intervals of different satellite systems represents a significant fundamental uncertainty in biomass burning characterization. Furthermore, even at the satellite sampling times, errors of omission or commission do occur, imposing another layer of uncertainty. These uncertainties related to non-observation of existing fires or false alarms on nonexistent fires, typically quantified in terms of errors of omission and commission, respectively, have been quite extensively investigated in the literature [e.g., *Ichoku et al*., 2003; *Li et al*., 2003; *Morisette et al*., 2005; *Csiszar et al*., 2006, 2014; *Schroeder et al*., 2008; *Freeborn et al*., 2014]. Therefore, this study focuses on uncertainties of measured parameters of actually observed fires, burned areas, and smoke constituents.

The objective of this study is to investigate uncertainties associated with the satellite characterization of biomass burning, as they relate to the derived geophysical

products such as smoke constituents and their applications. These uncertainties will be examined in the context of the 12 basic relevant questions outlined above. To anchor this study to contemporary reality, the analysis will be limited to satellite observation systems that are currently (or have been recently) operational, and known to provide data products that are related to biomass burning (Table 14.1). Then, we will explore how the observation uncertainties can propagate when used in deriving smoke emissions as well as in regional modeling. The conclusions will include an outlook on the potential for integration of available airborne and ground-based measurements to improve results.

14.2. METHODS

Satellite measurements related to biomass burning may be categorized into five groups of parameters, namely: active fires, burned surfaces, smoke plume dispositions, aerosol distribution and particle properties, and trace gas concentrations [*Ichoku et al*., 2012]. Whereas parameters of "active fires" (i.e., fire location, fire temperature and area, and fire radiative power [FRP]) and those of "burned surfaces" (i.e., burned area and burn severity proxy indices such as the differenced normalized burn ratio [dNBR]) are uniquely retrievable from satellite measurements within the limitations of remote sensing uncertainties [e.g., *Roy et al*., 2006, 2008; *French et al*., 2008; *Roy and Boschetti*, 2009; *Freeborn et al*., 2011; *Randerson et al*., 2012; *Hyer et al*., 2013; *Miettinen et al*., 2013; *Mouillot et al*., 2014], direct satellite retrieval of smoke constituents is somewhat more ambiguous because they are often mixed with similar particulate and gaseous constituents from nonfire sources [e.g., *Deeter et al*., 2003; *Kaufman et al*., 2005]. Therefore, at regional to global scales, the most frequent use of satellite active-fire and burned-area products is for the estimation of smoke emissions, which are subsequently applied to various uses, including air quality and climate modeling [e.g., *Heald et al*., 2003; *Kasischke and Bruhwiler*, 2003; *Kukavskaya et al*., 2013].

The amount of a specific carbonaceous aerosol or trace gas species emitted as a smoke constituent is traditionally derived as follows [e.g., *Lavoué et al*., 2000; *Andreae and Merlet*, 2001]:

$$M_x = EF_x * M_{biomass} \tag{14.1}$$

where M_x is the mass of the emitted smoke constituent x, EF_x is its emission factor, and $M_{biomass}$ is the mass of the dry biomass burned. $M_{biomass}$ can be estimated as follows [*Seiler and Crutzen*, 1980]:

$$M_{biomass} = A \times B \times \alpha \times \beta \tag{14.2}$$

where A is the burned area, B is the biomass density, α is the fraction of aboveground biomass, and β is the fraction consumed or combustion completeness.

Typically, EF_x is derived from laboratory or field experimentation, whereas A, B, α, and β are derived through satellite or airborne remote sensing, though they can be based on hybrid approaches. Although most current global and regional models employ emissions derived on the basis of equations (14.1) and (14.2), there are numerous uncertainties associated with this approach, particularly with regard to the accuracy of determination of the constituent parameters: EF_x A, B, α, and β, as well as the error propagation that results when they are combined [e.g., *French et al*., 2004].

In an effort to alleviate the complexity imposed by requiring the solution of equation (14.2) as a prerequisite to solving equation (14.1), *Ichoku and Kaufman* [2005] established a similar relationship to equation (14.1), in which EF_x is replaced with C_e^x, which is designated as the emission coefficient (for any given smoke constituent x), and $M_{biomass}$ is replaced with either fire radiative energy (*FRE*) or its release rate R_{fre} (i.e., *FRP*). Thus,

$$\begin{aligned} M_x &= C_e^x \cdot FRE \\ &\text{or} \\ R_x &= C_e^x \cdot R_{fre} \end{aligned} \tag{14.3}$$

where R_x is the rate of emission of species x (expressed in kg/s) since R_{fre} is the *FRE* release rate expressed in MJ/s, or MW. C_e^x is therefore expressed in kg/MJ. The validity of the relationship in equation (14.3) has been verified in a laboratory experiment, where satellite measurements of fire energetics and smoke were replicated by burning small biomass fuel samples in a burn chamber equipped with a giant smoke stack upon which the relevant instruments were set up, and the retrieved FRP and AOD were used to derive C_e for smoke aerosols [*Ichoku et al*., 2008b].

Based on equation (14.3), a new emissions dataset, known as the fire energetics and emissions research version 1.0 (FEERv1), has been developed from Terra- and Aqua-MODIS measurements of FRP and AOD [*Ichoku and Ellison*, 2014]. FEER.v1 is composed of a global gridded C_e^x dataset at 1° × 1° grid spatial resolution for smoke aerosols and a number of other important constituents. These gridded C_e^x values for smoke aerosols were applied to equation (14.3) together with FRE data obtained through time integration of MODIS FRP measurements that have been gridded at 0.5° × 0.5° resolution within the Global Fire Assimilation System [GFASv1.0; *Kaiser et al*., 2012]. The resulting daily emissions of smoke aerosols are then utilized as input into the Weather Research and Forecasting coupled with

Table 14.1 Selected Current or Recent Satellite Sensors Providing Observations of Fires and Smoke That Are Relevant to This Study

Satellie/sensor name	Description	Spatial resolution	Period	Reference (e.g.)
Quickbird	High-resolution satellite-borne sensors	2–4 m	2001–present	*Barbosa et al.* [2014]
Ikonos	High-resolution satellite-borne sensors	4 m	1999–present	*Barbosa et al.* [2014]
Landsat	Satellite series carrying the Thematic Mapper (TM) or enhanced TM (ETM) sensors	30 m	1979–present	*Chander et al.* [2009]
ASTER	Advanced Spaceborne Thermal Emission and Reflection Radiometer	15 m, 30 m, 90 m	1999–present	*Abrams*, [2000]
MODIS	Moderate-resolution Imaging Spectro-radiometer aboard Terra and Aqua	0.25 km, 0.5 km, 1 km	1999–present 2002–present	*Xiong et al.* [2009]
VIIRS	Visible–Infrared Imaging Radiometer Suite on the Suomi National Polar-Orbiting Partnership (NPP) satellite	375 m, 750 m	2011–present	*Hillger et al.* [2013]
BIRD	Bi-spectral Infra-Red Detection on a German Space Agency (DLR) small satellite	185 m, 370 m	2001–2004	*Lorentz et al.* [2013]
TET-1	Technologie Entwicklungstraeger on a German Space Agency (DLR) small satellite	42.4 m, 356 m	2012–present	*Lorentz et al.* [2013]
CALIOP	Cloud-Aerosol Lidar with Orthogonal Polarization on the Cloud-Aerosol Lidar and Infrared Pathfinder Satellite Observations (CALIPSO) satellite	5 km	2006–present	*Winker et al.* [2009]
MISR	Multi-angle Imaging Spectro-Radiometer aboard Terra	0.275 km, 1.1 km	1999–present	*Diner et al.* [2005]
AVHRR	Advanced Very High Resolution Radiometer	1 km	1978–present	*Ichoku et al.* [2003]
SPOT-VGT	The VEGETATION sensor aboard the European SPOT-4 satellite	1 km	1998–present	*Tansey et al.* [2004]
GOES	Sensors aboard the Geostationary Operational Environmental Satellite series	4 km	1994–present	*Zhang and Kondragunta* [2008]
SEVIRI	Spinning Enhanced Visible and Infrared Imager aboard the European Meteosat	3 km	2004–present	*Roberts and Wooster* [2008]
MOPITT	Measurements of Pollution in the Troposphere aboard the Terra satellite	22 km	1999–present	*Deeter et al.* [2003]
AIRS	Atmospheric Infrared Sounder aboard the Aqua satellite	90 km	2002–present	*Warner et al.* [2007]
TES	Tropospheric Emission Spectrometer aboard the Aura satellite	5×8 km	2004–present	*Luo et al.* [2007]
SCIA	SCIAMACHY on the European ENVISAT	30×120 km	2003–present	*Buchwitz et al.* [2006]
GOSAT	Greenhouse Gases Observing Satellite	10.5 km	2009–present	*Yokota et al.* [2009]

Note: The cited reference for each is just an example and not necessarily the official reference.

Chemistry (WRF-Chem) regional model for simulation of biomass burning aerosol emissions and dispersion over the NSSA region [*Zhang et al*., 2014]. The WRF-Chem AOD simulations are compared against MODIS-derived AOD for January and February 2010.

14.3. RESULTS AND DISCUSSION

Uncertainties associated with satellite measurements can vary widely because fires occur in different ecosystems at various scales under a diversity of conditions. Table 14.2 provides a summary of uncertainties associated with some of the satellite-based measurements of fire- and smoke-related variables, as obtained from literature, classified according to the 12 essential questions identified in the introduction, and expressed under different ranges of sensor spatial resolutions (very high: 0.001–0.01 km, high: 0.01–0.1 km, medium: 0.1–1 km, coarse: 1–10 km, and very coarse: 10–100 km), for ease of reference. These sensor-resolution classifications were determined based on a reasonable assessment of typical contemporary satellite instruments used for regional-global remote sensing. The reported uncertainty value ranges represent rough averages (not actual arithmetic means) estimated from the variety of values and plots published in the respective cited references. Overall, it is noticeable that uncertainties not only differ by variable but also by resolution, generally getting worse the coarser the resolution, as can be observed in cases represented in at least two spatial resolution categories. From the partial distribution of values in Table 14.2, it is obvious that most of the variables related to active fires and burned areas are observed at medium to coarse resolutions, whereas those associated with smoke are observed at coarse to very coarse resolutions. Analysis of global fire distributions has shown that lower FRP fires (which can be either relatively small hot fires or cooler fires of various sizes) occur much more frequently than larger ones in virtually all regions of the world [e.g., *Ichoku et al*., 2008a]. Thus, most fire-related variables are observed at resolutions that are much coarser than their scale of occurrence, thereby contributing to the uncertainty. Also, because of the temporally discrete nature of satellite observations, time-dependent fire and emissions characteristics such as fire duration, smoke emission rates, and transformations are not directly retrieved, though when the fires are large enough to be observed from geostationary satellites, it may be possible to determine fire duration. Otherwise, such time-dependent phenomena are typically derived through postproduction modeling that incorporates additional parameters from other sources.

One of the outcomes of the survey in Table 14.2 is that all satellite retrievals are subject to significantly large uncertainties (underestimation and overestimation). However, at each scale, fire radiative power (FRP) appears to be more prone to underestimation relative to higher resolutions [*Wooster et al*., 2003; *Roberts and Wooster*, 2008]. Burned area (BA) also appears to have a greater tendency toward underestimation [e.g., *Roy and Boschetti*, 2009]. This is probably because of the relatively coarse resolutions at which they are observed, causing nondetection of smaller or less intense fires and smaller burned areas [e.g., *Wang et al*., 2009; *Tsela et al*., 2014]. Since FRP and BA are the satellite-retrieved variables that are most commonly used for emissions estimates as in equations (14.2) and (14.3), the implications of their uncertainties for emissions require evaluation. Part of the reason why FRP and BA can be severely underestimated is because of the imaging geometry constraints of most satellite sensors, whereby pixels become large, fewer, and sometimes overlap away from nadir, resulting in lower total FRP, as illustrated in Figure 14.1. Similarly, BA has the tendency toward underestimation, whether it is derived using a change detection approach [e.g., *Roy et al*., 2008] or estimated from the active fire-pixel counts [e.g., *Giglio et al*., 2009]. A global assessment of the overall effect of this phenomenon based on a long record (2003–2009) of MODIS active fire observations in relation to scan angles is illustrated in Figure 14.2. By comparing fires observed at a single pixel at different off-nadir scan angles (starting from 25° up to the MODIS maximum of 55°) to the corresponding nadir pixel counts for the same fire, it has been found that a single fire pixel observed by MODIS at 55° off nadir can be equivalent to up to 16 fire pixels observed at nadir. In terms of FRP, although the value can be doubled at 55° off nadir, it becomes less than 30% when evaluated per km^2, which amounts to a net underestimation, since there are considerably fewer observations off nadir than at nadir.

To evaluate the uncertainty of aerosol emission estimates on model simulations, FEERv1 aerosol emissions were implemented in WRF-Chem over the NSSA region. Recent results of comparisons between FEERv1 aerosol emissions against other major emissions inventories in this region show that FEERv1 emissions are higher (by up to a factor of two) than many of the commonly used global fire emissions inventories that are based on bottom-up approaches [*Ichoku and Ellison*, 2014; *Zhang et al*., 2014]. Those bottom-up emissions inventories are typically used with enhancement factors in model simulations of smoke aerosols to match observed atmospheric aerosol distributions [e.g., *Kaiser et al*., 2012]. However, even when provided with uniform emissions, different models also have intrinsic characteristics that can significantly affect the uncertainty of simulations of smoke aerosol processes, transport, and impacts [e.g., *Textor et al*., 2007]. The quantitative evaluation performed in this study involves deriving aerosol optical depth (AOD)

Table 14.2 The Uncertainty Ranges of Satellite-Derived Fire and Smoke Variables

				Uncertainty levels*					
				Spatial resolution	Very high (0.001–0.01 km)	High (0.01–0.1 km)	Medium (0.1–1 km)	Coarse (1–10 km)	Very coarse (10–100 km)
Item no.	Essential questions	Satellite retrieved variable	Symbol	Satellite sensors**	QuickBird, Ikonos	Landsat, ASTER, SPOT, (Lidar/SAR)#	MODIS[a] VIIRS, BIRD, TET-1, CALIP	MODIS[a] MISR, AVHRR, SPOT-VGT, GOES, SEVIRI	MOPITT, AIRS, TES, SCIA, GOSAT
1	Fire location	Fire location	FL[b]			~0.15 km	~0.75 km	~5 km	
2	Fuel load and conditions	Biomass	BM[c]		±50%	±50%			
3	Fire size/intensity	Fire Area	FA[d]				65–250%	±50%	
		Fire Temp	FT[e]				±30%	±100 K	
		Fire Radiative Power	FRP[f]				±30%	±50%	
4	Fire characteristics (flaming/ smoldering)	Flaming ratio	FSR[g]				40%–140%		
5	Fire duration	N/A							
6	Burned area	Burned area	BA[h]			±10%	±20%	±30%	
		Burn Severity	BS[i]			±70%			
7	Smoke emission rate	N/A							
8	Plume injection height	Plume top height	PTH[j]					±0.5 km	
		Plume vertical profile	PVP[k]				±7%		
9	Major smoke constituents	Aerosol Optical Depth	AOD[l]					±0.15	
		Carbon Monoxide	CO[m]						±50%
		Carbon Dioxide	CO_2[n]						97%–102%
		Methane	CH_4[o]						96%–102%

10	Smoke transformation	N/A
11	Fire behavior	N/A
12	Fire diurnal/seasonal cycles	N/A

* Uncertainty levels are expressed in measurement units or percentages. In the case of the latter, the measured value is 100%, such that the range shows average uncertainty range.

** These are only selected currently or recently orbiting satellite sensors that are relevant to this study, and the details and relevant reference for each are given in Table 14.1.

[#] This represents a variety of spaceborne and airborne Lidar and synthetic aperture radar (SAR) systems that is used to estimate biomass (Period: variable, Res: 5–60 km) [e.g., *Montesano et al.*, 2014].

[a] MODIS currently offers spatial resolutions of: 0.5 km for BA, 1 km for FL and FRP, and 3–10 km for AOD.

[b] Location uncertainty depends on spatial resolution and observation geometry. These are expressed here as approximately half the typical average nominal pixel size in each resolution group. See *Zhukov et al*. [2006], *Hyer and Reid* [2009], *Csiszar et al*. [2014], *Schroeder et al*. [2014a,b].

[c] Biomass (BM) is used as a generic designation for fuel load. Airborne radar shows potential for spaceborne radar. See *Brandis and Jacobson* [2003], *Jin et al*. [2012].

[d] Uncertainty range in % about the mean estimates. See *Lorenz et al*. [2013], *Peterson et al*. [2013], *Peterson and Wang* [2013], *Giglio and Kendall* [2001].

[e] Uncertainty range in % about the mean estimates or in actual temperature (K) values. See *Lorenz et al*. [2013], *Giglio and Kendall* [2001].

[f] FRP is retrieved from satellite, but what is really needed in subpixel fire intensity. See *Kaufman et al*. [1998], *Wooster* [2003], *Zhukov et al*. [2006], *Roberts and Wooster* [2008, 2014], *Peterson et al*. [2013], *Peterson and Wang* [2013].

[g] See *Lorenz et al*. [2013].

[h] See *Loboda et al*. [2007], *Giglio et al*. [2009], *Roy and Boschetti* [2009], *Tsela et al*. [2010, 2014], *Stroppiana et al*. [2012], *Padilla et al*. [2014].

[i] BS is typically expressed in the form of differenced Normalized Burn Ratio (dNBR) or Relative dNBR (RdNBR); See *Epting et al*. [2005], *Miller and Thode* [2007].

[j] See *Scollo et al* [2012].

[k] Because of its curtain character, CALIOP seldom scans near smoke plume source, which is where it is most needed to characterize plume injection. See *Winker et al*. [2009, 2013], *Kacenelenbogen et al*. [2014].

[l] AOD is retrieved from satellite, but what is really needed is particulate matter (PM) concentrations in smoke. Typical range of AOD values is 0–5 (unitless). See *Petrenko and Ichoku* [2013].

[m] See *Kasibhatla et al*. [2002], *Kopacz* [2010].

[n] What is actually evaluated is dry air column-averaged mole fractions of CO2 (XCO2). See *Schneising et al*. [2008], *Morino et al*. [2011], *Reuter et al*. [2011].

[o] See *Schneising et al*. [2009], *Morino et al*. [2011].

N/A = parameters that are currently not directly retrieved from satellite measurements.

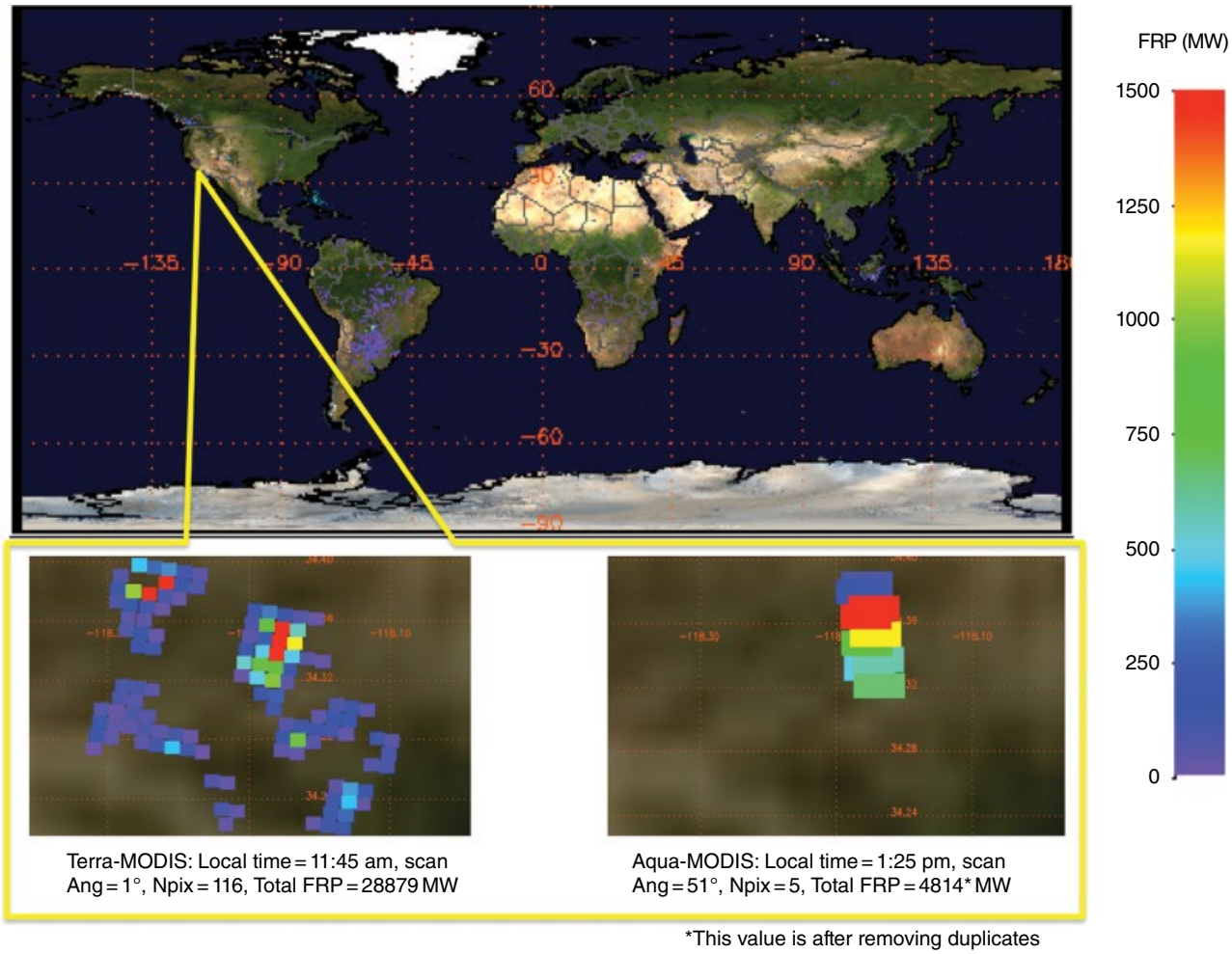

Figure 14.1 Effect of scan angle on MODIS observation of the Station Fire in Pasadena, California, on 30 August 2009. Fire detections near nadir (bottom left) show pixels to be almost square shaped at 1 × 1 km resolution, whereas near scan edge (bottom right) pixels are much fewer, individually stretched almost up to 4 × 2.5 km resolution, duplicated, and overlapping one another, and total FRP is underestimated.

from WRF-Chem based on FEERv1 emissions and comparing this with direct AOD retrievals from MODIS. This is done for January and February 2010, which is the typical peak of the burning season in NSSA. Incidentally, significant dust emissions also occur in this region during this season, as indicated by very heavy aerosol loading that appears prominently in dark red colors in Figure 14.3b, which represents a simple combination of both Terra- and Aqua-MODIS Collection 5 (C5) AOD retrievals from the Dark Target, Deep Blue, and Ocean algorithms. Although the current MODIS Collection 6 (C6) AOD product has a combined version [e.g., *Levy et al.*, 2013], C5 is used for the current comparison to avoid an attempt to characterize additional discrepancy due to version differences, as the FEERv1 emissions were based on C5. Since WRF-Chem simulations did not include dust emissions, to avoid (or at least limit) dust influence in the satellite AOD samples, it was decided that these comparisons would be most realistic at areas that are not in the normal seasonal dust trajectory. Four areas were selected for the MODIS/WRF-Chem AOD comparisons and labeled according to the main country or region covered, namely: Senegal, Gabon, Central Africa, and Southern Sudan (Figs. 14.3b and 14.3c). Terra- and Aqua-MODIS C5 AOD are in general good agreement overall, but WRF-Chem AOD simulations are very low (Fig. 14.3d), in spite of the fact that the FEERv1 emissions upon which they are based are higher than those of most other existing smoke emissions inventories. This AOD underestimation may be due to a combination of multiple factors, one of which may be emissions underestimation, while others may include WRF-Chem model variables and parameters as well as assumptions and process treatment algorithms. Also, although the main areas

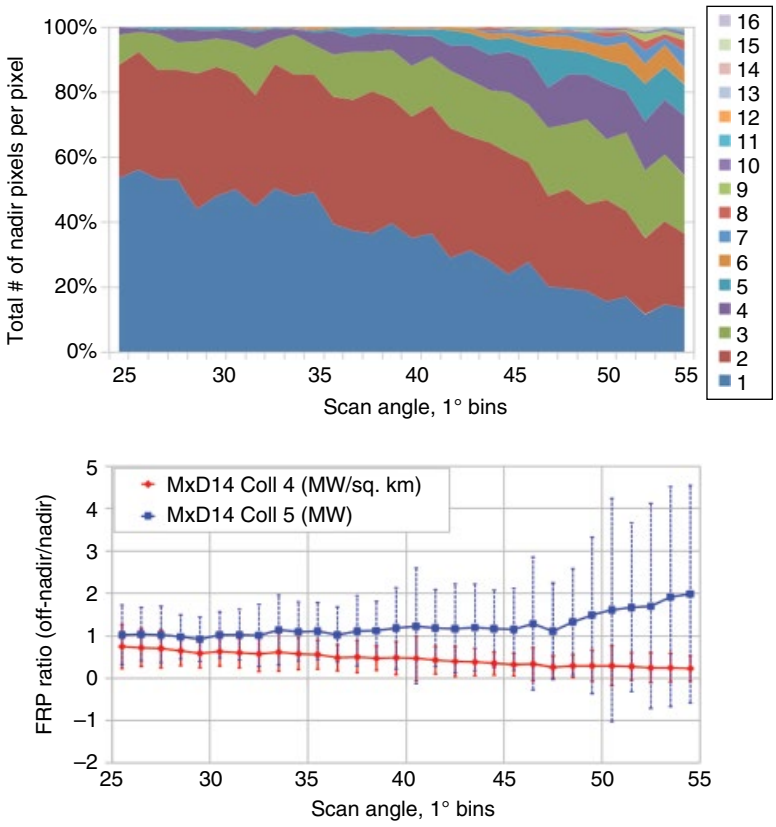

Figure 14.2 Analysis of the effect of scan angle on collocated MODIS fire observation from Terra and Aqua, within 20 min of each other globally for 2003–2009. This collocation is only possible within the high latitudes (>55°N) where there is significant overlap of MODIS swaths between the two satellites. MxD14 represents the official MODIS fire products from Terra (MOD14) and Aqua (MYD14). There were 11,295 pairs of Terra/Aqua fire observations. (Top) Relative percentages of off-nadir single pixel fire detection from one satellite and corresponding number of near-nadir pixels of the same fire from the other satellite. (Bottom) Ratios of the FRP value of single off-nadir pixels to total FRP value of the corresponding near-nadir fire pixels, expressed both in terms of FRP (as in MODIS collection 5) and FRP per unit area (as in MODIS collection 4). The point values are the means of such ratios for bins of 1° off-nadir observations starting at 25° scan angle, whereas error bars are the corresponding standard deviations of the FRP ratios.

of dust loading have been avoided in these comparisons, there could still be some residual dust or even cloud contamination in the MODIS-retrieved AOD. Because of various types of AOD retrieval constraints and MODIS swath coverage limitations, typical maps of AOD contain significant data gaps, such that the boxes for the regions of interest are seldom completely filled, as exemplified by Figure 14.3b, unlike Figure 14.3c, which shows complete coverage offered by the model. In Figure 14.3d, different circle symbol sizes on the Terra and Aqua curves depict the degree of coverage of sample areas for the MODIS AOD curves. The plots show that WRF-Chem AOD tends to agree better when the sample boxes have higher coverage by MODIS retrievals, as the root mean square error (RMSE) values denote in Table 14.3. Based on these results, it can be inferred that WRF-Chem regional modeling of smoke aerosols over NSSA using the FEERv1 satellite-based emissions estimates produce a net underestimation of AOD relative to satellite AOD, with the discrepancy becoming larger as the gap in satellite AOD coverage increases.

14.4. CONCLUSIONS

Satellite fire observation is relied upon for many applications. However, significant uncertainty is incurred in the satellite retrieval or estimation of biomass burning quantities, such as active fire location, area, temperature, radiative power, burned area and burn severity, plume injection and profile, and smoke constituents including aerosols and trace gases. Typically, the uncertainties tend to increase as the spatial and temporal resolutions of the

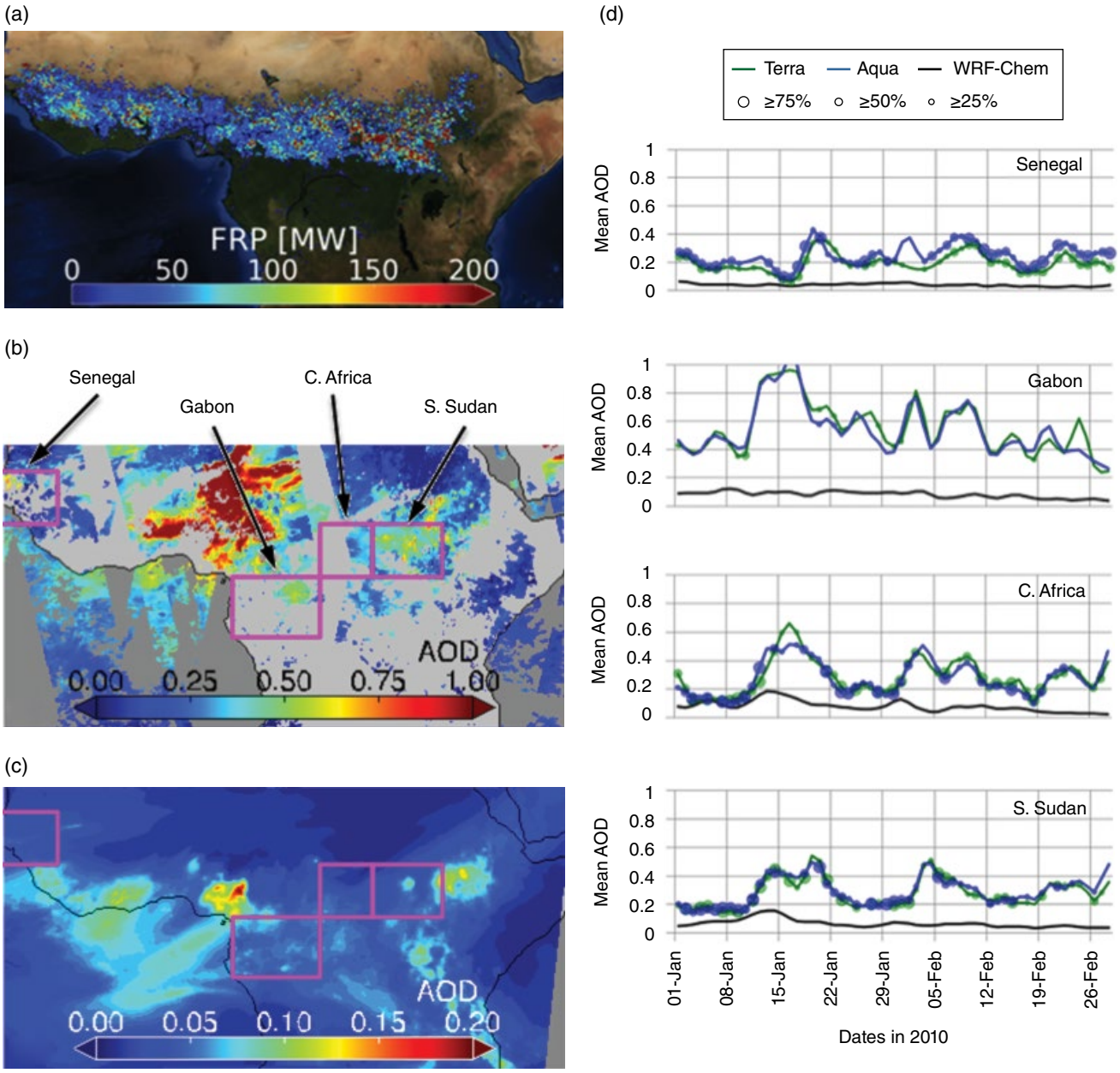

Figure 14.3 Evaluation of uncertainty in aerosol optical depth (AOD) generated from WRF-Chem model based on FEERv1 aerosol emissions, by comparison to satellite-observed AOD over northern sub-Saharan Africa (NSSA) during January–February 2010: (a) Fire locations and associated FRP values from MODIS on Terra and Aqua; (b) composited Terra and Aqua MODIS mean AOD for 5 February 2010, showing boxes where AOD comparisons are made; (c) WRF-Chem simulation of only smoke aerosol AOD for 5 February 2010, also showing the sampling box locations. AOD values increase from blue to red. Notice the difference in AOD value ranges as indicated by the color scales between (b) and (c). Boxed areas are selected to avoid the main dust trajectory (as indicated by the dark-red thick aerosol plume in [b]), such that the sampled AOD may be mainly smoke aerosols; (d) daily MODIS average AOD at Terra and Aqua overpass times (colored curves) and corresponding WRF-Chem simulations (black curves) for 12–1 p.m. local time, which coincides approximately with the average of the local times of Terra and Aqua overpasses. The size of the circles on the satellite-AOD curves indicate the extent of spatial coverage of the satellite retrievals within the sample boxes, as gaps do occur due to cloud or other factors that can cause AOD retrieval to fail (as seen in [b]).

Table 14.3 Root Mean Square Error (RMSE) Values Between WRF-Chem AOD Simulations and MODIS AOD Retrievals for Terra and Aqua According to Bins of 25% Coverage of MODIS AOD Retrievals Over Each Sample Box Area Shown in Figure 14.3b.

	Senegal		Gabon		C. Africa		S. Sudan	
Box coverage (cov.)	Terra	*Aqua*	*Terra*	*Aqua*	*Terra*	*Aqua*	*Terra*	*Aqua*
75% < = cov. <100%	– (0)	0.22 (16)	– (0)	– (0)	0.13 (20)	0.13 (13)	0.20 (20)	0.20 (12)
50% < = cov. <75%	0.17 (27)	0.20 (20)	0.27 (1)	– (0)	0.24 (14)	0.20 (13)	0.20 (17)	0.20 (19)
25% < = cov. <50%	0.18 (25)	0.25 (17)	0.39 (11)	0.47 (2)	0.29 (13)	0.25 (21)	0.29 (14)	0.25 (15)
0% < = cov. <25%	0.13 (7)	0.24 (6)	0.53 (47)	0.49 (56)	0.31 (11)	0.29 (12)	0.27 (8)	0.33 (13)

Note: The numbers in parentheses represent the sample size (i.e., the number of days in January–February 2010 falling within the respective coverage bins for each case).

satellite observations decrease. Incidentally, most of these biomass-burning quantities are currently observed at suboptimal spatial and temporal resolutions. For instance, the current operational systems, such as MODIS and VIIRS, that provide the most commonly used active fire products, observe these fires at nominal 1000 m and dual (375 m and 750 m) spatial resolutions, respectively, even though most open fires exist at much smaller scales. As a result, most of these fires are omitted and the FRP for those that are observed are mostly underestimated. In the same way, burned areas are underestimated. Since FRP and burned areas are used mostly to estimate smoke emissions, these also become underestimated and are propagated into modeling simulations of smoke distributions from fires.

Although such uncertainties affect fire measurements and modeling everywhere, the northern sub-Saharan African (NSSA) region has been used as a case study to evaluate the effect of emissions uncertainty on aerosol estimates for this study. This is fitting, given that NSSA contributes 20%–25% of global biomass burning, and together with southern sub-Saharan Africa (SSSA) make up > 50% of the annual global biomass burning. Nevertheless, NSSA biomass burning has been one of the least investigated by means of ground-based or airborne measurement techniques, and therefore potentially harbors the largest uncertainty, as estimates of its biomass burning parameters are based mainly on satellite observations and other proxy information. Overall, it is found that FEERv1 emissions, which are based on a top-down approach from MODIS measurements of FRP and AOD, when used in regional smoke modeling with the WRF-Chem model can underestimate AOD relative to MODIS by 0.13 to 0.27 RMSE in AOD when MODIS has AOD retrievals in 50% or more of the area of interest. Paradoxically, a similar comparison of MODIS C5 AOD against simulated AOD from the Goddard Chemistry Aerosol Radiation and Transport (GOCART) global model using emissions based on satellite BA products through a variety of bottom-up approaches show a severe overestimation in the NSSA region [*Petrenko et al.*, 2012]. This is even more surprising because those bottom-up emissions based on BA had been shown to produce lower smoke emissions than FEERv1, which is based on a top-down approach using FRP measurements [*Ichoku and Ellison*, 2014]. This type of obvious discrepancy causes a general confusion regarding which of the following three areas could be the main source of the uncertainty: emissions, model, or geographic region.

Uncertainties in the quantification of fire output, particularly smoke, by satellite and modeling can be affected by a variety of factors, including: satellite measurement characteristics, parameter retrieval algorithms, contamination of desired variables by other undesired targets such as clouds, model assumptions and resolution, and the surface and atmospheric characteristics of the geographic region of study. There is need for a well-coordinated, comprehensive, and robust strategy to address such uncertainty. Based on the results of the current study and those cited here, the following three recommendations become appropriate: (1) Conduct integrated field experiments combining ground-based, airborne, and satellite measurements and linking them to modeling in a synergistic way [e.g., *Schroeder et al.*, 2014a] to better characterize biomass burning energetics and emissions in a coherent manner. (2) Conduct such integrated field studies in the NSSA region, which contributes 20%–25% of global biomass burning emissions and even a larger proportion of atmospheric dust loading within the same season, making remote-sensing discrimination of dust and smoke almost impossible over land, and thus far investigated mainly over ocean [e.g., *Kaufman et al.*, 2005; *Guo et al.*, 2013]. (3) Design future fire-related satellite missions with specific attention toward significantly improving the spatial, temporal, spectral, and radiometric resolutions of sensors to maximize the retrieval of the various variables related to fires and smoke, as listed in Table 14.2, in order to optimally address their associated essential questions.

ACKNOWLEDGMENTS

This research was funded by NASA under its Research Opportunities in Space and Earth Sciences (ROSES), 2009 and 2013 Interdisciplinary Studies (IDS) Program (Dr. Jack Kaye, Earth Science Research Director), through the Radiation Sciences Program Managed by Dr. Hal Maring.

REFERENCES

Abrams, M. (2000), The Advanced Spaceborne Thermal Emission and Reflection Radiometer (ASTER): Data products for the high spatial resolution imager on NASA's Terra platform, *Int. J. Remote Sens.*, *21*(5), 847–859.

Andreae, M. O. (1991), Biomass burning: Its history, use, and distribution and its impact on environmental quality and global climate, 3–21, in *Global Biomass Burning: Atmospheric, Climatic, and Biospheric Implications*, edited by J. S. Levine, MIT Press, Cambridge, Massachusetts.

Andreae, M. O., and P. Merlet, (2001), Emission of trace gases and aerosols from biomass burning, *Glob. Biogeochem. Cycles*, *15*, 955– 966.

Barbosa, J. M., E. N. Broadbent, and M. D. Bitencourt (2014), Remote sensing of aboveground biomass in tropical secondary forests: A review, *Int. J. For. Res.*, 2014.

Brandis, K., and C. Jacobson (2003), Estimation of vegetative fuel loads using Landsat TM imagery in New South Wales, Australia, *Int. J. Wildland Fire*, *12*(2), 185–194.

Buchwitz, M., R. De Beek, S. Noël, J. P. Burrows, H. Bovensmann, O. Schneising, I. Khlystova, M. Bruns, H. Bremer, P. Bergamaschi, S. Komer, and M. Heimann (2006), Atmospheric carbon gases retrieved from SCIAMACHY by WFM-DOAS: Version 0.5 CO and CH 4 and impact of calibration improvements on CO 2 retrieval, *Atmos. Chem. Phys.*, *6*(9), 2727–2751.

Chander, G., B. L. Markham, and D. L. Helder (2009), Summary of current radiometric calibration coefficients for Landsat MSS, TM, ETM+, and EO-1 ALI sensors, *Remote Sens. Environ.*, *113*(5), 893–903.

Cohen, J. (2010), The wildland-urban interface fire problem, *Fremontia*, *16*.

Colarco, P. R., M. R. Schoeberl, B. G. Doddridge, L. T. Marufu, O. Torres, and E. J. Welton (2004), Transport of smoke from Canadian forest fires to the surface near Washington, D.C.: Injection height, entrainment, and optical properties, *J. Geophys. Res.*, *109*, D06203; doi:10.1029/2003JD004248.

Csiszar, I., J. Morisette, and L. Giglio (2006), Validation of active fire detection from moderate-resolution satellite sensors: The MODIS example in Northern Eurasia, *IEEE Trans. Geosci. Remote Sens.*, 1757–1764; doi:10.1109/TGRS.2006.875941.

Csiszar, I., W. Schroeder, L. Giglio, E. Ellicott, K. P. Vadrevu, C. O. Justice, and B. Wind (2014), Active fires from the Suomi NPP Visible Infrared Imaging Radiometer Suite: Product status and first evaluation results, *J. Geophys. Res. Atmos.*, *119*, 803–816; doi:10.1002/2013JD020453.

Deeter, M. N., L. K. Emmons, G. L. Francis, D. P. Edwards, J. C. Gille, J. X. Warner, B. Khattatov, D. Ziskin, J.-F. Lamarque, S.-P. Ho, V. Yudin, J.-L. Attie, D. Packman, J. Chen, D. Mao, and J. R. Drummond (2003), Operational carbon monoxide retrieval algorithm and selected results for the MOPITT instrument, *J. Geophys. Res. Atmos.*, *108*(D14), 1984–2012; doi: 10.1029/2002JD003186.

de Groot, W. J., R. Landry, W. A. Kurz, K. R. Anderson, P. Englefield, R. H. Fraser, R. J. Hall E. Banfield, D. A. Raymond, V. Decker, T. J. Lynham, and J. M. Pritchard (2007), Estimating direct carbon emissions from Canadian wildland fires, *Int. J. Wildland Fire*, *16*, 593–606; doi:10.1071/WF06150.

Diner, D. J., B. H. Braswell, R. Davies, N. Gobron, J. Hu, Y. Jin, R. A. Kahn, Y. Knyazikhin, N. Loeb, J.-P. Muller, A. W. Nolin, B. Pinty, C. B. Schaaf, G. Seiz, and J. Stroeve (2005), The value of multiangle measurements for retrieving structurally and radiatively consistent properties of clouds, aerosols, and surfaces, *Rem. Sens. Environ.*, *97*, 495–518.

Epting J., D. Verbyla, and B. Sorbel (2005), Evaluation of remotely sensed indices for assessing burn severity in interior Alaska using Landsat TM and ETM+, *Remote Sens. Environ.*, *96*(3–4), 328–339.

Freeborn, P. H., M. J. Wooster, and G. Roberts (2011), Addressing the spatiotemporal sampling design of MODIS to provide estimates of the fire radiative energy emitted from Africa, *Remote Sens. Environ.*, *115*(2), 475–489; doi:10.1016/j.rse.2010.09.017.

Freeborn, P. H., M. J. Wooster, G. Roberts, and W. Xu (2014), Evaluating the SEVIRI fire thermal anomaly detection algorithm across the Central African Republic using the MODIS active fire product, *Remote Sens.*, *6*, 1890–1917.

French, N. H. F., E. S. Kasischke, R. J. Hall, K. A. Murphy, D. L. Verbyla, E. E. Hoy, and J. L. Allen (2008), Using Landsat data to assess fire and burn severity in the North American boreal forest region: An overview and summary of results, *Int. J. Wildland Fire*, *17*(4), 443–462; doi:10.1071/WF08007.

French, N. H. F., et al. (2011), Model comparisons for estimating carbon emissions from North American wildland fire, *J. Geophys. Res.*, *116*, G00K05; doi:10.1029/2010JG001469.

French, N. H. F., P. Goovaerts, and E. S. Kasischke (2004), Uncertainty in estimating carbon emissions from boreal forest fires, *J. Geophys. Res.*, *109*, D14S08; doi:10.1029/2003JD003635.

Gatebe, C. K., C. M. Ichoku, R. Poudyal, M. O. Román, and E. Wilcox (2014), Surface albedo darkening from wildfires in northern sub-Saharan Africa, *Environ. Res. Lett.*, *9*(6), 065003.

Giglio, L., and J. D. Kendall (2001), Application of the Dozier retrieval to wildfire characterization: A sensitivity analysis, *Remote Sens. Environ.*, *77*(1), 34–49. doi:10.1016/S0034-4257(01)00192-4.

Giglio, L., J. T. Randerson, G. R. Van der Werf, P. S. Kasibhatla, G. J. Collatz, D. C. Morton, and R. S. DeFries (2010), Assessing variability and long-term trends in burned area by merging multiple satellite fire products, *Biogeosciences*, *7*(3), 1171–1186.

Giglio, L., T. Loboda, D. P. Roy, B. Quayle, and C. O. Justice (2009), An active-fire based burned area mapping algorithm for the MODIS sensor, *Remote Sens. Environ.*, *113*(2), 408–420. doi:10.1016/j.rse.2008.10.006.

Guo, Y., B. Tian, R. A. Kahn, O. Kalashnikova, S. Wong, and D. E. Waliser (2013), Tropical Atlantic dust and smoke aerosol variations related to the Madden-Julian Oscillation in MODIS and MISR observations, *J. Geophys. Res. Atmos.*, *118*, 4947–4963; doi:10.1002/jgrd.50409.

Heald, C. L., D. J. Jacob, P. I. Palmer, M. J. Evans, G. W. Sachse, H. B. Singh, and D. R. Blake (2003), Biomass burning emission inventory with daily resolution: Application to aircraft observations of Asian outflow, *J. Geophys. Res.*, *108*(D21), 8811; doi:10.1029/2002JD003082.

Henderson, S. B., M. Brauer, Y. C. MacNab, and S. M. Kennedy (2011), Three measures of forest fire smoke exposure and their associations with respiratory and cardiovascular health outcomes in a population-based cohort, *Environ. Health Pers.*, *119*(9), 1266.

Hillger, D., T. Kopp, T. Lee, D. Lindsey, C. Seaman, S. Miller, J. Solbrig, S. Kidder, S. Bachmeier, T. Jasmin, and T. Rink (2013), First-Light Imagery from Suomi NPP VIIRS, *Bull. Amer. Meteor. Soc.*, *94*, 1019–1029. doi: 10.1175/BAMS-D-12-00097.1.

Hyer, E. J., and J. S. Reid (2009), Baseline uncertainties in biomass burning emission models resulting from spatial error in satellite active fire location data, *Geophys. Res. Lett.*, *36*, L05802; doi:10.1029/2008GL036767.

Hyer, E. J., J. S. Reid, E. M. Prins, J. P. Hoffman, C. C. Schmidt, J. I. Miettinen, and L. Giglio (2013), Patterns of fire activity over Indonesia and Malaysia from polar and geostationary satellite observations, *Atmos. Res.*, *122*, 504–519.

Ichoku, C., and L. Ellison (2014), Global top-down smoke-aerosol emissions estimation using satellite fire radiative power measurements, *Atmos. Chem. Phys.*, *14*(13), 6643–6667; doi:10.5194/acp-14-6643-2014.

Ichoku, C., and Y. J. Kaufman (2005), A method to derive smoke emission rates from MODIS fire radiative energy measurements, *IEEE Trans. Geosci. Remote Sens.*, *43*(11), 2636–2649.

Ichoku, C., J. V. Martins, Y. J. Kaufman, M. J. Wooster, P. H. Freeborn, W. M. Hao, S. Baker, C. A. Ryan, and B. L. Nordgren (2008b), Laboratory investigation of fire radiative energy and smoke aerosol emissions, *J. Geophys. Res.*, *113*, D14S09; doi:10.1029/2007JD009659.

Ichoku, C., L. Giglio, M. J. Wooster, and L. A. Remer (2008a), Global characterization of biomass-burning patterns using satellite measurements of Fire Radiative Energy, *Remote Sens. Environ.*, *112*, 2950–2962.

Ichoku, C., R. Kahn, and M. Chin (2012), Satellite contributions to the quantitative characterization of biomass burning for climate modeling, *Atmos. Res.*, *111*, 1–28.

Ichoku, C., Y. J. Kaufman, L. Giglio, Z. Li, R. H. Fraser, J.-Z. Jin, and W. M. Park (2003), Comparative analysis of daytime fire detection algorithms using AVHRR data for the 1995 fire season in Canada: Perspective for MODIS, *Int. J. Remote Sens.*, *24*(8), 1669–1690.

Jin, S., and S.-C. Chen (2012) Application of QuickBird imagery in fuel load estimation in the Daxinganling region, China, *Int. J. Wildland Fire*, *21*(5), 583–590.

Kacenelenbogen, M., J. Redemann, M. A. Vaughan, A. H. Omar, P. B. Russell, S. Burton, R. R. Rogers, R. A. Ferrare, and C. A. Hostetler (2014), An evaluation of CALIOP/CALIPSO's aerosol-above-cloud detection and retrieval capability over North America, *J. Geophys. Res. Atmos.*, *119*, 230–244; doi:10.1002/2013JD020178.

Kaiser, J. W., et al. (2012), Biomass burning emissions estimated with a global fire assimilation system based on observations of fire radiative power, *Biogeosciences*, *9*, 527–554; doi:10.5194/bg-9-527-2012.

Kasibhatla, P., A. Arellano, J. A. Logan, P. I. Palmer, and P. Novelli (2002), Top-down estimate of a large source of atmospheric carbon monoxide associated with fuel combustion in Asia, *Geophys. Res. Lett.*, *29*(19), 6–1.

Kasischke, E. S., and L. M. Bruhwiler (2003), Emissions of carbon dioxide, carbon monoxide and methane from boreal forest fires in 1998, *J. Geophys. Res.*, *107*, 8146; doi:10.1029/2001JD000461.

Kaufman, Y. J., C. O. Justice, L. P. Flynn, J. D. Kendall, E. M. Prins, L. Giglio, D. E. Ward, W. P. Menzel, and A. W. Setzer (1998), Potential global fire monitoring from EOS-MODIS, *J. Geophys. Res. Atmos.*, *103*(D24), 32215–32238.

Kaufman, Y. J., O. Boucher, D. Tanré, M. Chin, L. A. Remer, and T. Takemura (2005), Aerosol anthropogenic component estimated from satellite data, *Geophys. Res. Lett.*, *32*, L17804; doi:10.1029/2005GL023125.

Kopacz, M., D. J. Jacob, J. A. Fisher, J. A. Logan, L. Zhang, I. A. Megretskaia, R. M. Yantosca, K. Singh, D. K. Henze, J. P. Burrows, M. Buchwitz, I. Khlystova, W. W. McMillan, J. C. Gille, D. P. Edwards, A. Eldering, V. Thouret, and P. Nedelec (2010), Global estimates of CO sources with high resolution by adjoint inversion of multiple satellite datasets (MOPITT, AIRS, SCIAMACHY, TES), *Atmos. Chem. Phys.*, *10*(3), 855–876; doi:10.5194/acp-10-855-2010.

Kukavskaya, E. A., A. J. Soja, A. P. Petkov, E. I. Ponomarev, G. A. Ivanova, and S. G. Conard (2013), Fire emissions estimates in Siberia: evaluation of uncertainties in area burned, land cover, and fuel consumption, *Can. J. For. Res.*, *43*(5), 493–506; doi:10.1139/cjfr-2012-0367.

Lavoué, D., C. Liousse, H. Cachier, B. J. Stocks, and J. G. Goldammer (2000), Modeling of carbonaceous particles emitted by boreal and temperate wildfires at northern latitudes, *J. Geophys. Res.*, *105*(D22), 26,871–26,890; doi:10.1029/2000JD900180.

Levy, R. C., S. Mattoo, L. A. Munchak, L. A. Remer, A. M. Sayer, and N. C. Hsu (2013), The Collection 6 MODIS aerosol products over land and ocean, *Atmos. Meas. Tech. Discuss.*, *6*, 159–259.

Li, Z., R. Fraser, J. Jin, A. A. Abuelgasim, I. Csiszar, P. Gong, R. Pu, and W. M. Hao (2003), Evaluation of algorithms for fire detection and mapping across North America from satellite, *J. Geophys. Res.*, *108*(D2), 4076; doi:10.1029/2001JD001377.

Loboda, T., K. J. O'Neal, and I. Csiszar (2007), Regionally adaptable dNBR-based algorithm for burned area mapping

from MODIS data, *Remote Sens. Environ.*, *109*(4), 429–442. doi:10.1016/j.rse.2007.01.017.

Lorenz, E. (2013), Thermal remote sensing with small satellites: BIRD, TET and the next generation BIROS, 149–176, in *Thermal Infrared Remote Sensing*, Springer Netherlands.

Luo, M., C. P. Rinsland, C. D. Rodgers, J. A. Logan, H. Worden, S. Kulawik, A. Eldering, A. Goldman, M. W. Shephard, M. Gunson, and M. Lampel (2007), Comparison of carbon monoxide measurements by TES and MOPITT: Influence of a priori data and instrument characteristics on nadir atmospheric species retrievals, *J. Geophys. Res.*, *112*, D09303; doi:10.1029/2006JD007663.

Michalek, J. L., N. H. F. French, E. S. Kasischke, R. D. Johnson, and J. E. Colwell (2000), Using Landsat TM data to estimate carbon release from burned biomass in an Alaskan spruce complex, *Int. J. Remote Sens.*, *21*, 323–338.

Miettinen, J., E. Hyer, A. S. Chia, L. K. Kwoh, S. C. and Liew (2013), Detection of vegetation fires and burnt areas by remote sensing in insular Southeast Asian conditions: current status of knowledge and future challenges, *Int. J. Remote Sens.*, *34*(12), 4344–4366.

Miller, J. D., and A. E. Thode (2007), Quantifying burn severity in a heterogeneous landscape with a relative version of the delta Normalized Burn Ratio (dNBR), *Remote Sens. Environ.*, *109*(1), 66–80; doi:10.1016/j.rse.2006.12.006.

Montesano, P. M., R. F. Nelson, R. O. Dubayah, G. Sun, Bruce D. Cook, K. J. R. Ranson, E. Næsset, and V. Kharuk (2014), The uncertainty of biomass estimates from LiDAR and SAR across a boreal forest structure gradient, *Remote Sens. Environ*., *154*, 398–407.

Moody, J. A., R. A. Shakesby, P. R. Robichaud, S. H. Cannon, D. A. Martin (2013), Current research issues related to post-wildfire runoff and erosion processes, *Earth Sci. Rev*., *122*, 10–37.

Morino, I., O. Uchino, M. Inoue, Y. Yoshida, T. Yokota, P. O. Wennberg, G. C. Toon, D. Wunch, C. M. Roehl, J. Notholt, T. Warneke, J. Messerschmidt, D. W. T. Griffith, N. M. Deutscher, V. Sherlock, B. Connor, J. Robinson, R. Sussmann, and M. Rettinger (2011), Preliminary validation of column-averaged volume mixing ratios of carbon dioxide and methane retrieved from GOSAT short-wavelength infrared spectra, *Atmos. Meas. Tech.*, *4*, 1061–1076; doi:10.5194/amt-4-1061-2011.

Morisette, J. T., L. Giglio, I. Csiszar, and C. O. Justice (2005), Validation of MODIS active fire detection product over Southern Africa using ASTER data, *Int. J. Remote Sens.*, *26*(19), 4239–4264.

Mouillot, F., M. G. Schultz, C. Yue, P. Cadule, K. Tansey, P. Ciais, and E. Chuvieco (2014), Ten years of global burned area products from spaceborne remote sensing, a review: Analysis of user needs and recommendations for future developments, *Int. J. Appl. Earth Obs. Geoinf.*, *26*, 64–79.

Padilla, M., S. V. Stehman, and E. Chuvieco (2014), Validation of the 2008 MODIS-MCD45 global burned area product using stratified random sampling, *Remote Sens. Environ*., *144*, 187–196; doi:10.1016/j.rse.2014.01.008.

Peterson, D., and J. Wang (2013), A Sub-pixel-based calculate of fire radiative power from MODIS observations: 2. Sensitivity analysis and potential fire weather application, *Remote Sens. Environ*., *129*, 231–249.

Peterson, D., J. Wang, C. Ichoku, E. Hyer, and V. Ambrosia (2013), A sub-pixel-based calculation of fire radiative power from MODIS observations: 1. Algorithm development and initial assessment, *Remote Sens. Environ*., *129*, 262–279; doi:10.1016/j.rse.2012.10.036.

Petrenko, M., and C. Ichoku (2013), Coherent uncertainty analysis of aerosol measurements from multiple satellite sensors, *Atmos. Chem. Phys.*, *13*, 6777–6805; doi:10.5194/acp-13-6777-2013.

Petrenko, M., R. Kahn, M. Chin, A. Soja, T. Kucsera, and Harshvardhan (2012), The use of satellite-measured aerosol optical depth to constrain biomass burning emissions source strength in the global model GOCART, *J. Geophys. Res.*, *117*, D18212; doi:10.1029/2012JD017870.

Pouliot, G., T. G. Pace, B. Roy, T. Pierce, and D. Mobley (2008), Development of a biomass burning emissions inventory by combining satellite and ground-based information, *J. Appl. Remote Sens.*, *2*(1), 021501–021501.

Randerson, J. T., Y. Chen, G. R. van der Werf, B. M. Rogers, and D. C. Morton (2012), Global burned area and biomass burning emissions from small fires, *J. Geophys. Res.*, *117*, G04012; doi:10.1029/2012JG002128.

Reuter, M., et al. (2011), Retrieval of atmospheric CO2 with enhanced accuracy and precision from SCIAMACHY: Validation with FTS measurements and comparison with model results, *J. Geophys. Res.*, *116*, D04301; doi:10.1029/2010JD015047.

Roberts, G., and M. J. Wooster (2014), Development of a multi-temporal Kalman filter approach to geostationary active fire detection and fire radiative power (FRP) estimation, *Remote Sens. Environ*., *152*, 392–412.

Roberts, G., M. J. Wooster, G. L. W. Perry, N. Drake, L.-M. Rebelo, and F. Dipotso (2005), Retrieval of biomass combustion rates and totals from fire radiative power observations: Application to southern Africa using geostationary SEVIRI imagery, *J. Geophys. Res.*, *110*, D21111; doi:10.1029/2005JD006018.

Roberts, G. J., and M. J. Wooster (2008), Fire detection and fire characterization over Africa using Meteosat SEVIRI, *IEEE Trans. Geosci. Remote Sens.*, *46*(4), 1200–1218; doi:10.1109/TGRS.2008.915751.

Roy, D. P., and L. Boschetti (2009), Southern Africa validation of the MODIS, L3JRC and GLOBCARBON burned area products, *IEEE Trans. Geosci. Remote Sens.*, *47*(4), 1032–1044; doi:10.1109/TGRS.2008.2009000.

Roy, D. P., L. Boschetti, and S. N. Trigg (2006), Remote sensing of fire severity: assessing the performance of the normalized burn ratio, *Geosci. Remote Sens. Lett*., *IEEE*, *3*(1), 112–116.

Roy, D. P., L. Boschetti, C. O. Justice, and J. Ju, (2008), The collection 5 MODIS burned area product: Global evaluation by comparison with the MODIS active fire product, *Remote Sens. Environ.*, *112*(9), 3690–3707.

Roy, D. P., L. Boschetti, S. W. Maier, and A. M. S. Smith (2010), Field estimation of ash and char colour-lightness using a standard grey scale, *Int. J. Wildland Fire*, *19*(6), 698–704.

Schneising, O., M. Buchwitz, J. P. Burrows, H. Bovensmann, M. Reuter, J. Notholt, R. Macatangay, and T. Warneke (2008),

Three years of greenhouse gas column-averaged dry air mole fractions retrieved from satellite, Part 1: Carbon dioxide, *Atmos. Chem. Phys.*, *8* (14), 3827–3853.

Schneising, O., M. Buchwitz, J. P. Burrows, H. Bovensmann, P. Bergamaschi, and W. Peters (2009), Three years of greenhouse gas column-averaged dry air mole fractions retrieved from satellite, Part 2: Methane, *Atmos. Chem. Phys.*, *9*, 443–465; doi:10.5194/acp-9-443-2009.

Schroeder, W., E. Ellicott, C. Ichoku, L. Ellison, M. B. Dickinson, R. D. Ottmar, C. Clements, D. Hall, V. Ambrosia, and R. Kremens (2014a), Integrated active fire retrievals and biomass burning emissions using complementary near-coincident ground, airborne and spaceborne sensor data, *Remote Sens. Environ.*, *140*, 719–730.

Schroeder, W., E. Prins, L. Giglio, I. Csiszar, C. Schmidt, J. Morisette, and D. Morton (2008), Validation of GOES and MODIS active fire detection products using ASTER and ETM plus data, *Remote Sens. Environ.*, *112*, 2711–2726.

Schroeder, W., P. Oliva, L. Giglio, and I. A. Csiszar (2014b), The New VIIRS 375 m active fire detection data product: Algorithm description and initial assessment, *Remote Sens. Environ.*, *143*, 85–96.

Schultz, M. G., A. Heil, J. J. Hoelzemann, A. Spessa, K. Thonicke, J. G. Goldammer, A. C. Held, J. M. C. Pereira, and M. van het Bolscher (2008), Global wildland fire emissions from 1960 to 2000, *Glob. Biogeochem. Cycles*, *22*, GB2002; doi:10.1029/2007GB003031.

Scollo, S., R. A. Kahn, D. L. Nelson, M. Coltelli, D. J. Diner, M. J. Garay, and V. J. Realmuto (2012), MISR observations of Etna volcanic plumes, *J. Geophys. Res.*, *117*, D06210; doi:10.1029/2011JD016625.

Seiler W., and P. J. Crutzen (1980), Estimates of gross and net fluxes of carbon between the biosphere and the atmosphere from biomass burning, *Clim. Change*, *2*, 207– 248.

Stroppiana, D., G. Bordogna, P. Carrara, M. Boschetti, L. Boschetti, and P. A. Brivio (2012), A method for extracting burned areas from Landsat TM/ETM+ images by soft aggregation of multiple Spectral Indices and a region growing algorithm, *ISPRS J. Photogramm. Remote Sens.*, *69*, 88–102.

Tansey, K., J.-M. Grégoire, D. Stroppiana, A. Sousa, J. Silva, J. Pereira, L. Boschetti, et al. (2004),Vegetation burning in the year 2000: Global burned area estimates from SPOT VEGETATION data, *J. Geophys. Res. Atmos.*, *109*(D14), 1984–2012

Textor, C., M. Schulz, S. Guibert, S. Kinne, Y. Balkanski, S. Bauer, T. Berntsen, et al. (2007), The effect of harmonized emissions on aerosol properties in global models, an AeroCom experiment, *Atmos. Chem. Phys.*, *7*(17), 4489–4501.

Tsela, P., K. Wessels, J. Botai, S. Archibald, D. Swanepoel, K. Steenkamp, and P. Frost (2014), Validation of the two standard MODIS satellite burned-area products and an empirically-derived merged product in South Africa, *Remote Sens.*, *6*(2), 1275–1293; doi:10.3390/rs6021275.

Tsela, P. L., P. van Helden, P. Frost, K. Wessels, and S. Archibald (2010), Validation of the MODIS burned-area products across different biomes in South Africa, 3652–3655, in 2010 *IEEE International Geoscience and Remote Sensing Symposium, IEEE*; doi:10.1109/IGARSS.2010.5650253.

van der Werf, G. R., J. T. Randerson, L. Giglio, G. J. Collatz, M. Mu, P. S. Kasibhatla, D. C. Morton, R. S. DeFries, Y. van Jin, and T. T. van Leeuwen (2010), Global fire emissions and the contribution of deforestation, savanna, forest, agricultural, and peat fires (1997–2009), *Atmos. Chem. Phys.*, *10*(23), 11707–11735.

van der Werf, G. R., J. T. Randerson, L. Giglio, G. J. Collatz, P. S. Kasibhatla, and A. F. Arellano Jr. (2006), Interannual variability in global biomass burning emissions from 1997 to 2004, *Atmos. Chem. Phys.*, *6*, 3423–3441; doi:10.5194/acp-6-3523-2006.

Vermote, E., E. Ellicott, O. Dubovik, T. Lapyonok, M. Chin, L. Giglio, and G. J. Roberts (2009), An approach to estimate global biomass burning emissions of organic and black carbon from MODIS fire radiative power, *J. Geophys. Res.*, *114*, D18205; doi:10.1029/2008JD011188.

Wang, J., S. A. Christopher, U. S. Nair, J. S. Reid, E. M. Prins, J. Szykman, and J. L. Hand (2006), Mesoscale modeling of Central American smoke transport to the United States: 1. "Top-down" assessment of emission strength and diurnal variation impacts, *J. Geophys. Res.*, *111*, D05S17; doi:10.1029/2005JD006416.

Wang, W., Y. Liu, J. J. Qu, and X. Hao (2009), Analysis of the moderate resolution imaging spectroradiometer contextual algorithm for small fire detection, *J. Appl. Remote Sens.*, *3*(1), 031502–031502.

Warner, J., M. M. Comer, C. D. Barnet, W. W. McMillan, W. Wolf, E. Maddy, and G. Sachse (2007), A comparison of satellite tropospheric carbon monoxide measurements from AIRS and MOPITT during INTEX-A, *J. Geophys. Res.*, *112*, D12S17; doi:10.1029/2006JD007925.

Wiedinmyer, C., B. Quayle, C. Geron, A. Belote, D. McKenzie, X. Zhang, S. O'Neill, and K. K. Wynne (2006), Estimating emissions from fires in North America for air quality modeling, *Atmos. Environ.*, *40*, 3419–3432; doi:10.1016/j.atmosenv.2006.02.010.

Winker, D. M., J. L. Tackett, B. J. Getzewich, Z. Liu, M. A. Vaughan, and R. R. Rogers (2013), The global 3-D distribution of tropospheric aerosols as characterized by CALIOP, *Atmos. Chem. Phys.*, *13*, 3345–3361; doi:10.5194/acp-13-3345-2013.

Winker, D. M., M. A. Vaughan, A. Omar, Y. Hu, K. A. Powell, Z. Liu, W. H. Hunt, and S. A. Young (2009), Overview of the CALIPSO mission and CALIOP data processing algorithms, *J. Atmos. Oceanic Technol.*, *26*, 2310–2323; doi:10.1175/2009JTECHA1281.1.

Wooster, M. J. (2003), Fire radiative energy for quantitative study of biomass burning: derivation from the BIRD experimental satellite and comparison to MODIS fire products, *Remote Sens. Environ.*, *86*(1), 83–107; doi:10.1016/S0034-4257(03)00070-1.

Xiong, X., K. Chiang, J. Sun, W. L. Barnes, B. Guenther, and V. V. Salomonson (2009), NASA EOS Terra and Aqua MODIS on-orbit performance, *Adv. Space Res.*, *43*(3), 413–422.

Yokota, T., Y. Yoshida, N. Eguchi, Y. Ota, T. Tanaka, H. Watanabe, and S. Maksyutov (2009), Global concentrations of CO2 and CH4 retrieved from GOSAT: First preliminary results, *Sola*, *5*(0), 160–163.

Zhang, F., J. Wang, C. Ichoku, E. J. Hyer, Z. Yang, C. Ge, S. Su, X. Zhang, S. Kondragunta, J. W. Kaiser, C. Wiedinmyer, and A. da Silva (2014), Sensitivity of mesoscale modeling of smoke direct radiative effect to the emission inventory: a case study in northern sub-Saharan African region, *Environ. Res. Lett.*, *9*(7), 075002.

Zhang, X., and S. Kondragunta (2008), Temporal and spatial variability in biomass burned areas across the USA derived from the GOES fire product, *Remote. Sens. Environ.*, *112*, 2886–2897.

Zhukov, B., E. Lorenz, D. Oertel, M. Wooster, and G. Roberts (2006), Spaceborne detection and characterization of fires during the Bispectral Infrared Detection (BIRD) experimental satellite mission (2001–2004), *Remote Sens. Environ.*, *100*, 29–51.